ISSN 1070-3632, Russian Journal of General Chemistry, 2022, Vol. 92, No. 12, pp. 2832–2837. © Pleiades Publishing, Ltd., 2022.

Morphology and Luminescent Properties of Microcrystalline $NaYF_4$ Phosphors Doped with Terbium(III) Ions

A. A. Betina[a], T. S. Bulatova[a], I. E. Kolesnikov[a], N. A. Bogachev[a], M. Yu. Skripkin[a], and A. S. Mereshchenko[a,*]

[a] *St. Petersburg State University, St. Petersburg, 199034 Russia*
**e-mail: a.mereshchenko@spbu.ru*

Received August 29, 2022; revised August 29, 2022; accepted October 6, 2022

Abstract—New microcrystalline phosphors $NaY_{1-x}Tb_xF_4$ (x = 0–0.6) were obtained by the hydrothermal synthesis. All compounds have the hexagonal β-$NaYF_4$ crystalline phase. Terbium(III) ions isomorphically replace yttrium ions, which results in increasing the unit cell parameters and decreasing the particle size. The maximum luminescence intensity is observed for the $NaY_{0.6}Tb_{0.4}F_4$ compound.

Keywords: luminescence, rare earth elements, terbium, yttrium, microparticles, solid solutions

DOI: 10.1134/S1070363222120349

Crystalline micro- and nanomaterials containing ions of rare earth elements are the objects of numerous studies in inorganic chemistry and materials science [1, 2].

Such materials are widely studied due to their optical properties and broad application within such areas as the design of luminescent thermometers, photocatalysts, and the sensors of biologically important substances [3–5]. Among other compounds the special attention was paid to Ln^{3+}-doped β-$NaYF_4$ because of pronounced luminescence. The dependence of the luminescence intensity on the lanthanide concentration is usually nonmonotonic due to concentration quenching. Earlier, we studied the concentration effect of the luminescent rare-earth doping ion (Eu^{3+} and Er^{3+}) on the emission intensity in β-$NaYF_4$ materials [6, 7]. To continue this research, the effect of terbium concentration on the structure, morphology, and luminescent properties of $NaY_{1-x}Tb_xF_4$ microparticles was studied in the present work.

A series of $NaY_{1-x}Tb_xF_4$ (x = 0, 0.05, 0.1, 0.15, 0.2, 0.3, 0.4, 0.5, 0.6) compounds with different content of yttrium and terbium were synthesized for the study. Compounds $NaLnF_4$ can crystallize in two polymorphic forms, the cubic α-phase (metastable high-temperature phase) and the hexagonal β-phase (thermodynamically stable low-temperature phase). The hexagonal phase usually has a higher luminescence efficiency compared to the cubic phase [8]. According to XRD data all $NaY_{1-x}Tb_xF_4$ compounds synthesized in this work have the hexagonal β-$NaYF_4$ crystalline phase (Fig. 1): the exact coincidence of the diffraction maxima of the synthesized phosphors and the reference sample (β-$NaYF_4$, JCPDS No. 16-0334) is observed. Thus, Tb^{3+} ions are able to isomorphically replace Y^{3+} ions in the

Table 1. Refined unit cell parameters of the $NaY_{1-x}Tb_xF_4$ compounds

$x(Tb^{3+})$	a, Å	c, Å	V, Å^3
0.00	5.9902	3.5267	109.6
0.05	5.9911	3.5282	109.7
0.10	5.9943	3.5309	109.9
0.15	5.997	3.5336	110.1
0.20	5.997	3.5336	110.1
0.30	6.0009	3.5392	110.4
0.40	6.0031	3.5437	110.6
0.50	6.0048	3.5472	110.8
0.60	6.0089	3.5537	111.1

crystal lattice of the obtained compounds, which agrees with the well-known Goldschmidt rule, since the ion radii of terbium(III) (r_{ion} = 1.095 Å) and yttrium(III) (r_{ion} = 1.075 Å) for the coordination number nine [9, 10] differ only slightly (≈2%). The unit cell parameters of the compounds were refined from X-ray powder diffraction (XRD) patterns (Table 1).

The replacement of yttrium ions by larger terbium(III) ions leads to an increase in the unit cell parameters and volume. The linear dependence of the cell volume on the concentration of terbium ions (approximation confidence factor $R^2 = 0.99$) suggests that Vegard's law [11] is obeyed for this series of solid solutions.

The morphology of the obtained microcrystals was studied by scanning electron microscopy (SEM). We found that the samples consist of particles shaped as hexagonal prisms, and the replacement of yttrium by terbium ions does not affect the particle shape. (Figs. 2a–2f). The particles have a diameter from 75 to 580 nm. The average particle diameter decreases with an increase in the concentration of terbium ions (Fig. 3). A similar decrease in particle size resulting from lanthanide doping was previously observed for $NaY_{1-x}Eu_xF_4$ (x = 0–0.6) series [6]. We explain this phenomenon with the lanthanide radius effect on the crystal growth rate [12, 13]. A larger ionic radius corresponds to a lower density of positive charge on the surface of the crystal nucleus, which, in turn, leads to a decrease in the rate of the diffusion of negatively charged fluoride ions to the surface and, as a consequence, a lower particle growth rate and a smaller final particle size. The ionic radius of Tb^{3+} is greater than that of Y^{3+}, which leads to the lower growth rate and particle size of compounds containing terbium ions.

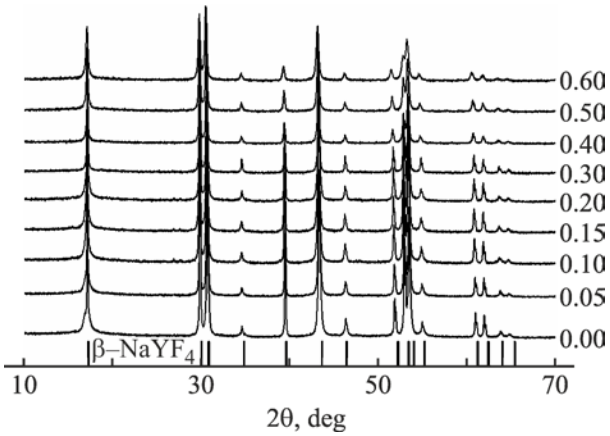

Fig. 1. XRD patterns of $NaY_{1-x}Tb_xF_4$ samples and relative intensities of β-$NaYF_4$ reflexes.

To select the excitation wavelength, the excitation spectrum was measured at the emission wavelength of 544 nm ($^5D_4$–$^7F_5$ transition). Characteristic emission maxima at 378 and 487 nm in the spectrum correspond to $^7F_6$–$^5D_3$ and $^7F_6$–$^5D_4$ transitions, respectively. The position of the peak maxima in the excitation spectra

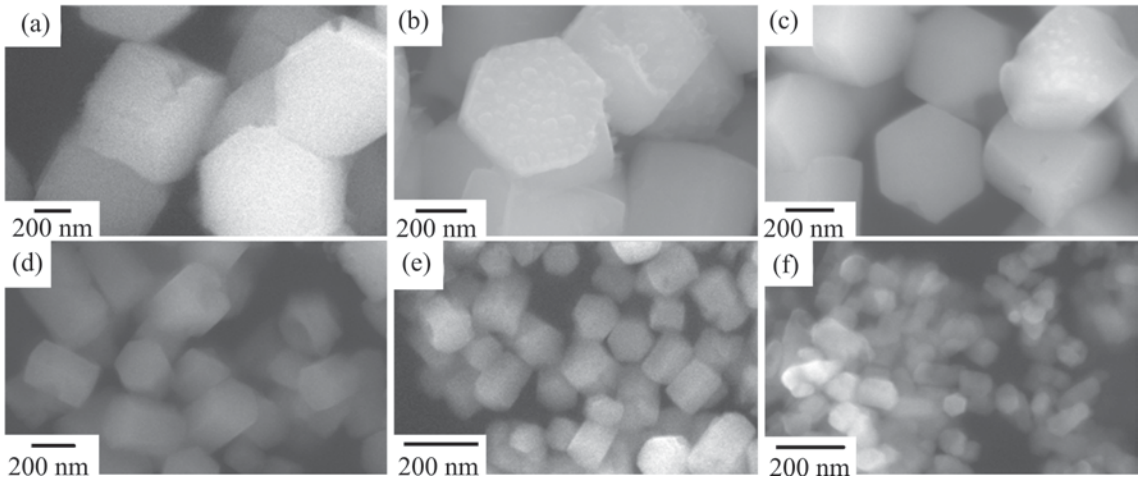

Fig. 2. SEM images of microcrystals: (a) $NaYF_4$, (b) $NaY_{0.9}Tb_{0.1}F_4$, (c) $NaY_{0.8}Tb_{0.2}F_4$, (d) $NaY_{0.7}Tb_{0.3}F_4$, (e) $NaY_{0.6}Tb_{0.4}F_4$, (f) $NaY_{0.4}Tb_{0.6}F_4$.

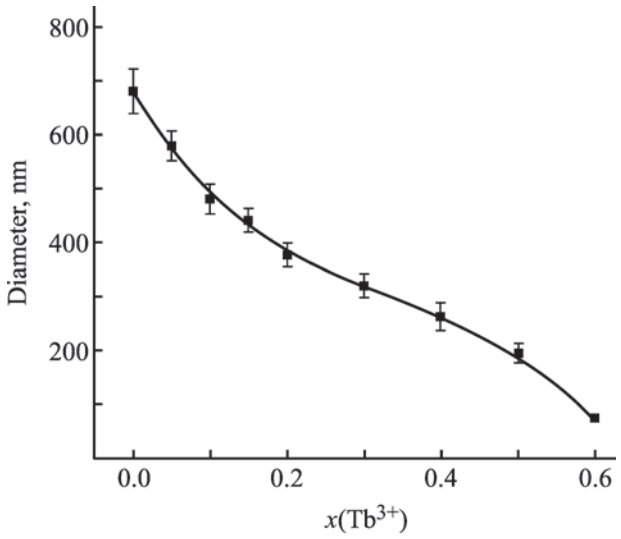

Fig. 3. Dependence of the average particle diameter on the terbium content in the $NaY_{1-x}Tb_xF_4$ samples.

does not depend on the Tb^{3+} concentration. For further study, the excitation wavelength of 378 nm was chosen (Fig. 4a) as the most intense band.

The emission spectra (Fig. 4b) contains sharp peaks attributed to the electron transitions inside the 4*f*-shell of terbium(III) ion, which correspond to electronic radiative transitions $^5D_4$–$^7F_6$ (489 nm), $^5D_4$–$^7F_5$ (544 nm), $^5D_4$–$^7F_4$ (585 nm), $^5D_4$–$^7F_3$ (620 nm), and $^5D_4$–$^7F_2$ (643 nm). The most prominent transition in the spectra is $^5D_4$–$^7F_5$ transition centred at 544 nm. It should be noted that the fine structure of the emission bands remains almost unchanged in the range $0.05 \le x \le 0.5$, which indicates that the local environment of Tb^{3+} does not change in this concentration range. The fine structure of the emission bands for $NaY_{0.4}Tb_{0.6}F_4$ is different from the other samples, which is probably due to local structural rearrangements in the Tb^{3+} environment, but in general does not lead to a change of the space group. The compound $NaY_{0.6}Tb_{0.4}F_4$ has the maximum intensity of the Stokes luminescence (Fig. 5a), whereas at higher content of terbium ions concentration quenching takes place.

The effect of the concentration of terbium(III) ions on the luminescence decay kinetics monitored at 544 nm ($^5D_4$–$^7F_5$ transition) upon 378 nm excitation (Fig. 5b). The luminescence decay lifetime corresponds to the lifetime of the $^5D_4$ state of the Tb^{3+} ion. The luminescence decay lifetime practically does not change in the range of terbium ion content of $0.05 \le x \le 0.2$. Further increase in the terbium(III) ions concentration results in a decrease in the lifetime. This is explained by the rather large distance between terbium(III) ions in the crystal lattice at the low concentration ($x \le 0.2$). The average distance between them decreases with an increase in the concentration

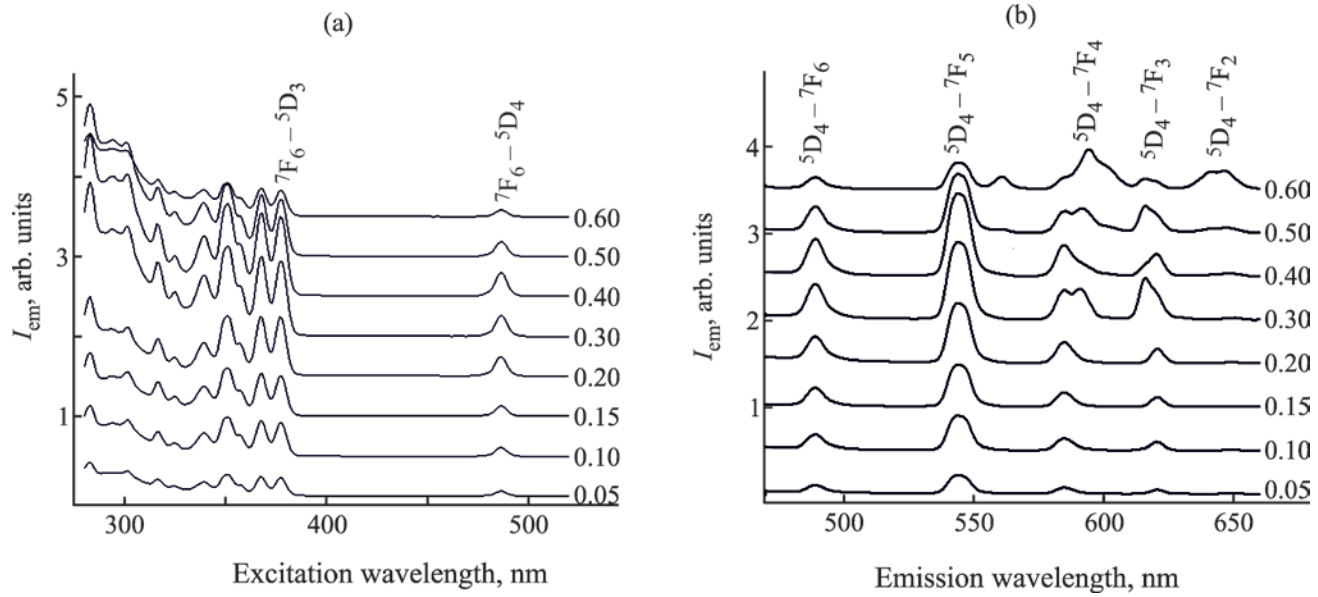

Fig. 4. (a) Excitation (λ_{em} = 544 nm) and (b) emission (λ_{ex} = 378 nm) spectra of $NaY_{1-x}Tb_xF_4$ samples.

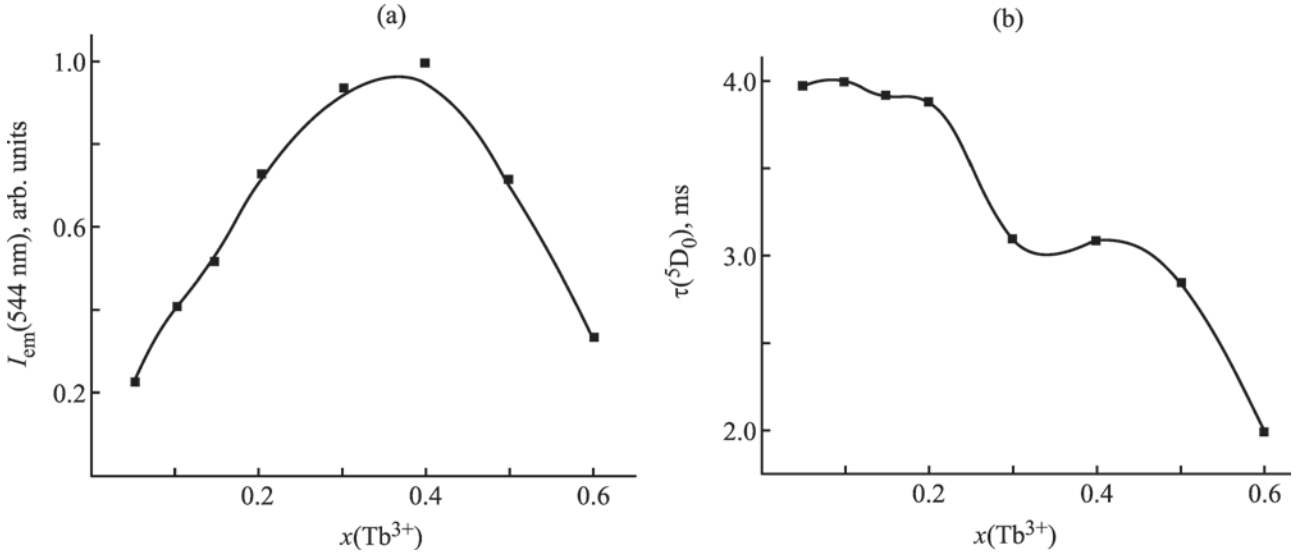

Fig. 5. The dependence of (a) peak luminescence intensity (λ_{ex} = 378 nm, λ_{lum} = 544 nm) and (b) luminescence decay lifetime on the terbium content.

of terbium ions, which leads to a significant increase in the efficiency of non-radiative processes due to the energy transfer from one terbium ion to another, and as a consequence, a decrease in the luminescence lifetime and intensity due to a decrease in quantum efficiency.

As a result of our research, we have clarified the mechanism of Stokes luminescence of terbium(III) ions in the $NaYF_4$ matrix (Fig. 6.). Upon 378 and 487-nm excitation, Tb^{3+} is promoted into excited electronic states corresponding to $^5D_3$ and $^5D_4$ levels, respectively. The main channel of relaxation from the $^5D_3$ level is internal conversion to the $^5D_4$ level, however, low-intensity radiative transitions from the $^5D_3$ level to ^7F_J levels of the ground state term are also observed. Direct excitation of the Tb^{3+} ion into the $^5D_4$ level is followed by radiative transitions to ^7F_J levels.

Thus, doping of $NaYF_4$ with terbium(III) ions results in the formation of solid solutions where Tb^{3+} isomorphically replaces yttrium ions, which leads to an increase in the unit cell parameters and a decrease in the particle size of the studied compounds. The $NaY_{1-x}Tb_xF_4$ compounds show luminescence in the range of compositions $0.05 \le x \le 0.5$ upon 378 and 487-nm excitation. The maximum intensity of Stokes luminescence is achieved for the compound $NaY_{0.6}Tb_{0.4}F_4$, whereas at higher contents of terbium ions concentration quenching is observed.

EXPERIMENTAL

The following reagents were used for the synthesis of phosphors: yttrium chloride hexahydrate and terbium chloride hexahydrate (99.9%, Chemcraft, Russia), chemically-pure grade citric acid, sodium hydroxide, ammonium fluoride, ethanol, copper(II) chloride, aqueous ammonia solution, murexide, and potassium bromide (Nevareaktiv, Russia), and Trilon B (standard 0.1 g-eq, Nevareaktiv, Russia).

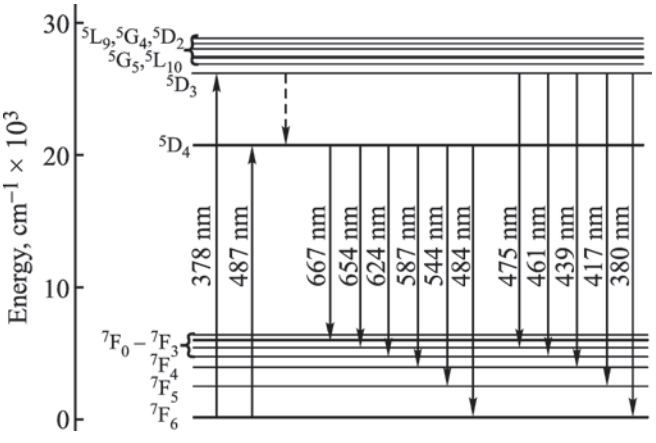

Fig. 6. Scheme of Stokes luminescence of Tb^{3+} ions in the $NaYF_4$ matrix.

All compounds were synthesized according to a previously developed technique [6]. As a source of yttrium and terbium ions, 0.3 M aqueous solutions of yttrium and terbium chlorides were used, which were previously standardized by the method of reverse titration of a Trilon B excess with nickel(II) chloride in the presence of an ammonia buffer (pH = 9) and murexide. To prepare reaction mixtures for hydrothermal synthesis, solutions of yttrium and terbium salts were mixed in the ratio corresponding to the stoichiometry of the synthesized compound, after which 1.8 mmol of citric acid was added to the resulting mixtures, and the volume was adjusted to 5 mL. The total content of rare earth element chlorides in the resulting mixtures was 0.75 mmol. To the resulting solutions, 2.5 mL of 3.6 M sodium hydroxide (9 mmol) was added drop by drop with intensive stirring, which lasted 15 min more. Then, 8 mL of a solution containing 11 mmol of ammonium fluoride and 11 mmol of sodium hydroxide was added to these solutions with stirring, and the resulting solution was left to mix for another 15 min. Next, the reaction mixture was placed in a sealed steel autoclave with a Teflon liner and kept for 17 h at 180°C. The suspension obtained after synthesis in the autoclave was transferred into centrifugation tubes and the resulting solid solutions were separated from the liquid phase in a centrifuge for 5 min at a rotor rotation speed of 4000 rpm. The white precipitate was separated by decantation, after which 3 mL of ethanol was added for washing, the precipitate was dispersed in ethanol using an ultrasonic bath or manually, and then separated again on a centrifuge. After that, the resulting precipitate was washed 3 times with water and dried in air for 24 h at 60°C. The composition of the obtained microcrystalline compounds was confirmed by the energy dispersion spectroscopy method.

The morphologies of microstructures of the synthesized samples were characterized using scanning electron microscopy (SEM) on a Zeiss Merlin electron microscope (Zeiss, Germany) using an energy-dispersive X-ray spectroscopy (EDX) module (Oxford Instruments INCAx-act, UK). X-ray powder diffraction (XRD) measurements were performed on a D2 Phaser (Bruker, USA) X-ray diffractometer using Cu Ka radiation (l = 1.54056 Å). The luminescence spectra were recorded on the Fluorolog-3 fluorescence spectrometer (Horiba JobinYvon, Japan) under equal conditions. To carry out quantitative photoluminescence studies, the synthesized samples (5 mg) and potassium bromide pre-calcined at 120°C (300 mg) were pressed into pellets.

AUTHOR INFORMATION

N.A. Bogachev, ORCID: http://orcid.org/0000-0002-9495-0669

I.E. Kolesnikov, ORCID: http://orcid.org/0000-0002-5051-4064

V.G. Nosov, ORCID: http://orcid.org/0000-0001-9817-0048

M.Yu. Skripkin, ORCID: http://orcid.org/0000-0001-9841-150X

E.M. Khairullina, ORCID: http://orcid.org/0000-0002-4699-5862

A.S. Mereshchenko, ORCID: http://orcid.org/0000-0001-9390-1446

ACKNOWLEDGMENTS

The measurements were performed at the Research Park of Saint-Petersburg State University (“Magnetic Resonance Research Centre,” “SPbU Computing Centre,” “Cryogenic Department,” “Interdisciplinary Resource Centre for Nanotechnology,” “Centre for X-ray Diffraction Studies,” “Chemical Analysis and Materials Research Centre,” and “Centre for Optical and Laser Materials Research”). This research was funded by Fellowship of President of Russia MD-1191.2022.1.3.

CONFLICT OF INTEREST

The authors declare no conflict of interest.

REFERENCES

1. Zheng, B., Fan, J., Chen, B., Qin, X., Wang, J., Wang, F., Deng, R., and Liu, X., *Chem. Rev.*, 2022, vol. 122, no. 6, p. 5519. https://doi.org/10.1021/acs.chemrev.1c00644
2. Chen, G., Qiu, H., Prasad, P.N., and Chen, X., *Chem. Rev*., 2014, vol. 114, no. 10, p. 5161. https://doi.org/10.1021/cr400425h
3. Swieten, T.P., Yu, D., Yu, T., Vonk, S.J.W., Suta, M., Zhang, Q., Meijerink, A., and Rabouw, F.T., *Adv. Opt. Mater*., 2021, vol. 9, no. 1, p. 2001518. https://doi.org/10.1002/adom.202001518
4. Tou, M., Mei, Y., Bai, S., Luo, Z., Zhanga, Y., and Li, Z., *Nanoscale*, 2016, vol. 8, no. 1, p. 553. https://doi.org/10.1039/c5nr06806a

5. Hu, J., Wang, R., Fan, R., Huang, Z., Liu, Y., Guo, G., and Fu, H., *J. Lumin*., 2020, vol. 217, p. 116812. https://doi.org/10.1016/j.jlumin.2019.116812
6. Kolesnikov, I.E., Vidyakina, A.A., Vasileva, M.S., Nosov, V.G., Bogachev, N.A., Sosnovsky, V.B., Skripkin, M.Y., Tumkin, I.I., Lahderanta, E., and Mereshchenko, A.S., *New J. Chem*., 2021, vol. 45, p. 10599. https://doi.org/10.1039/d1nj02193a
7. Vidyakina, A.A., Kolesnikov, I.E., Bogachev, N.A., Skripkin, M.Y., Tumkin, I.I., Lähderanta, E., and Mereshchenko, A.S., *Materials*, 2020, vol. 13, p. 3397. https://doi.org/10.3390/ma13153397
8. Wang, F. and Liu, X., *Account. Chem. Res*., 2014, vol. 47, no. 4, p. 1378. https://doi.org/10.1021/ar5000067
9. Shannon, R.D., *Acta Cryst. A*, 1976, vol. 32, p. 751. https://doi.org/10.1107/S0567739476001551
10. Szefczyk, B., Roszak, R., and Roszak, S., *RSC Adv*., 2014, vol. 4, no. 43, p. 22526. https://doi.org/10.1039/c4ra00211c
11. Denton, A.R. and Ashcroft, N.W., *Phys. Rev. A*, 1991, vol. 43, p. 3161. https://doi.org/10.1103/PhysRevA.43.3161
12. Wang, F., Han, Y., Lim, C.S., Lu, Y., Wang, J., Xu, J., Chen, H., Zhang, C., Hong, M., and Liu, X., *Nature*, 2010, vol. 463, p. 1061. https://doi.org/10.1038/nature08777
13. Damasco, J.A., Chen, G., Shao, W., Agren, H., Huang, H., Song, W., Lovell, J.F., and Prasad, P.N., *ACS Appl. Mater. Interfaces*, 2014, vol. 6, no. 16, p. 13884. https://doi.org/10.1021/am503288d